AUTOMATIC INSPECTION OF FE WELD DEFECTS

A.B. Aleksandrov[1], Yu.A. Zhukov[1], Yu.K. Karlov[1], V.V. Rozhkov[1], V.N. Vasyukov[2]
[1] JSC Novosibirsk Chemical Concentrates Plant, Russia, Novosibirsk;[2] NSTU, Russia, Novosibirsk

1. Introduction: Control of welding operation quality at final stages of production of VVER fuel elements (FE) for nuclear power plants in order to provide for leak-tightness of nuclear fuel is the most important factor of ensuring FE operational safety. Ultrasonic echo pulse method of non-destructive testing is considered as very promising. The available publications and numerous experiments of the authors are evidence of the fact that reliable registration of weld defects having dimensions of nearly dozens and even a few micrometers is possible at frequencies in the range of 15…50 MHz. Results of ultrasonic inspection are presented as a digital image. With increase of the resolution power of piezoelectric transducer the image self-descriptiveness increases and simultaneously the data volume grows up to about hundreds of megabytes per item. Visual inspection is practically impossible during series fabrication. Large-scale production requires automation of fuel element test process by means of computer analysis of ultrasonic images. The present paper describes some methods of automated FE weld defect detection and determination of defect dimensions and its location.

2. Description of ultrasonic NDT method based on computer information processing: Main weld defects are gas pores and incomplete penetration, i.e. discontinuity of root of weld. NDT is aimed at determination of defect existence (defect detection), measurement of defect dimensions and determination of defect location.

The present paper describes the results of studies made by the Central Research Laboratory of JSC "Novosibirsk Chemical Concentrate Plant" using the scanning ultrasonic device АКС7 «Fregat» (Fig.1).
Combined piezoelectric transducers 3, 21 of V375-SU type (Panametrics, Inc.), generate ultrasonic pulses with average frequency of 30 MHz. Longitudinal axes of piezoelectric transducers having a common plane with the longitudinal axis of the tested FE make 90^0 and 30^0 angles, respectively, with the normal to cylindrical surface. The tested FE is placed into distilled water. The distance between transducer and FE surface is equal to 18.7 mm. Since the object is in near zone of the transducer, it is impossible to measure the actual dimensions of weld defect on the basis of directional properties of transducer. The described methods make it possible to perform automated measurement of dimensions of defect images or conditional defect dimensions.

Each ultrasonic transducer scans the FE in two directions: along generating line of FE cylindrical surface (x axis of the used coordinate system) and along the guide line (y axis). This corresponds to FE rotation about its axis between x axis scanning cycles. Thus, the line scanning (line-to-line spacing about 20μm) is realized. While scanning along the generating line the ultrasonic transducer is periodically emitting pulses so that distance between the neighbour scans is about 20μm as well.

As a result of scanning by each transducer and time sampling of received oscillations with a sampling interval $T_d = 2$ ns (with sampling frequency $f_d = 500$ MHz), a three-dimensional array $d(k,m,n)$ of digital data is formed. This data array presents the intensity of received signal as a function of two space variables that can be determined by equations $x = k\Delta_x$, $y = m\Delta_y$, where $\Delta_x = \Delta_y = 20$ μm, and a time variable (signal delay $z = nT_d$). The three-dimensional array can be considered as a set of two-dimensional arrays of two types. A set of data $d(k,m,n = const)$ conforming to the same delay will be referred to as *layer* and a set of points $d(k,m = const,n)$ with equal values of the y coordinate will be referred to as *section*. It can be seen that the section corresponds to B-scan. In the selected experimental conditions the information array volume is equal to 160 - 750 Mbyte.

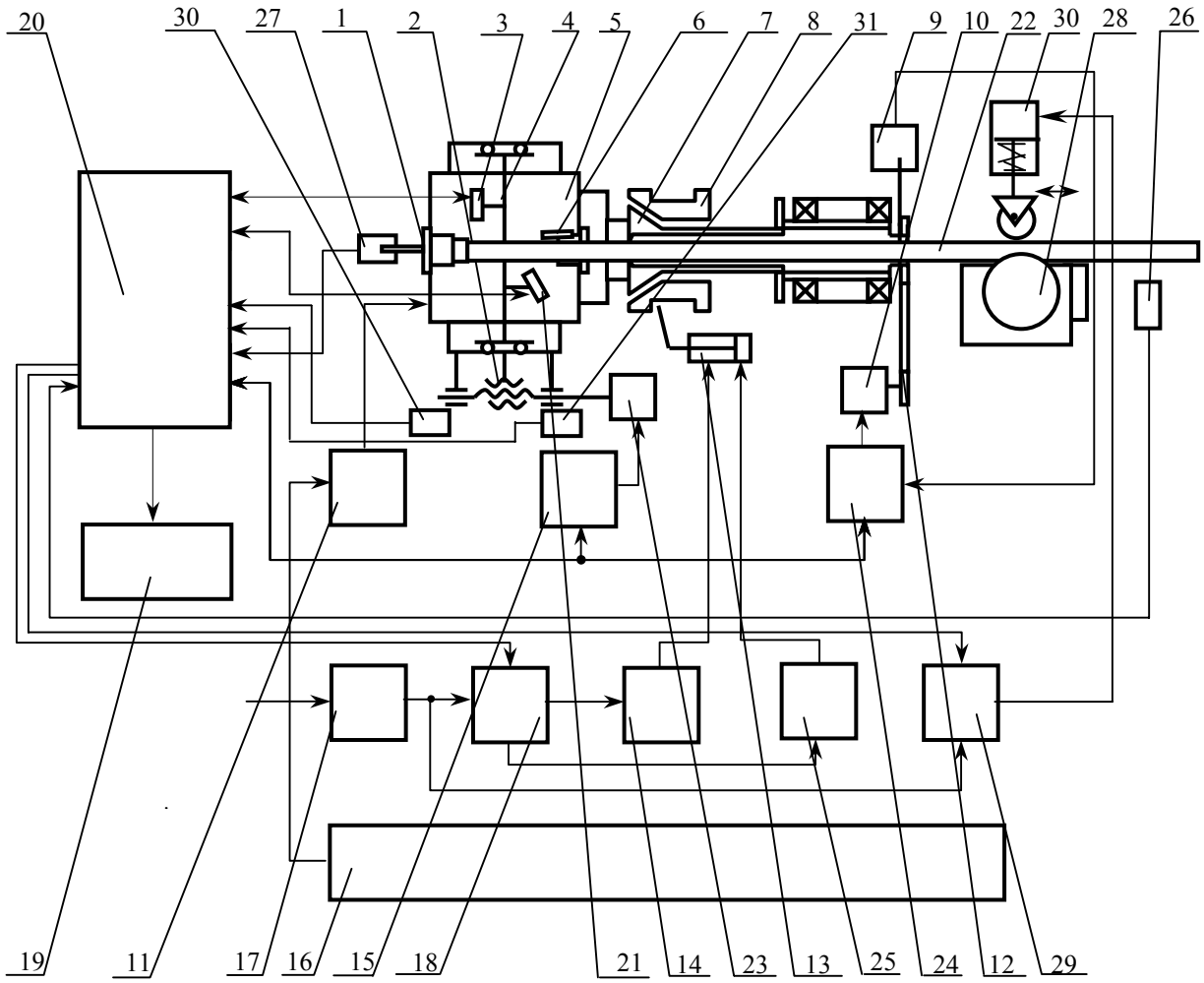

Fig. 1. *Functional diagram of installation*

1 – centering mount; 2 – screw pair; 3, 21 – piezo-electric transducer; 4 – carriage; 5 – weldpool; 6 – overflow valve; 7 – collet; 8 – bushing; 9 – «Initial/end position of rotational unit» sensor; 10 – step motor of clamping and rotational unit; 11 – pump; 12 – reducer (1:4); 13, 30 – air cylinder; 14, 25 – throttle; 15, 24 – step motor control unit ; 16 – control panel; 17 – air treatment unit; 18 – distributor; 19 – printer; 20 – Automated system of acoustic control, movement control and data processing; 22 – item; 23 – carriage step motor; 26 – «Item at the loading/unloading unit position» sensor; 27 – «Item in the control zone» sensor; 28 – loading/unloading unit; 29 – distributor (solenoid-operated pneumatic valve); 30 - «Carriage end position» sensor; 31 - «Carriage starting position» sensor.

Normal and oblique incidence sounding modes are used. Oblique incidence sounding has significant advantages as compared with normal sounding.

In case of normal sounding, echo pulses reflected from both the internal and external surfaces of FE cylindrical cladding significantly exceed the signals reflected from defects. This results in substantial masking of weld defects near the external surface. When oblique incidence sounding is used the level of signal reflected from the cylindrical surfaces decreases abruptly because the most part of reflected energy is not directed to ultrasonic transducer. An additional advantage of oblique sounding is a higher spatial resolution and a greater intensity of reflections of transverse ultrasonic waves from weld defects. The transverse waves are the main waves observed in zirconium during oblique sounding. The transverse waves have two times shorter length than longitudinal

waves (main waves during normal sounding). Moreover, during oblique sounding the effective reflection surface of incomplete penetration (a plane defect oriented perpendicularly to the FE axis) is greater than during normal sounding. This contributes to increase of the reflected signal intensity which results in increase of the probability of defect detection. Layers and sections of the array obtained during oblique FE sounding and the ones during normal sounding are shown in Fig. 2. The arrows connect images of the same defect, i.e. a pore.
Section obtained during normal sounding is characterized by existence of a large signal reflected from the external cylinder surface boundary. Alternating dark and light stripes (slant lines) are caused by oscillating nature of the signal. The signal reflected from the internal cylinder surface (bottom signal) the image of which is in the lower part of the section is weaker than the signal reflected from the external surface. The specific feature of the above signal is the absence of the reflected signal in the left part corresponding to monolithic portion of the end part. A significantly weaker signal corresponds to a pore image. Observability can be improved by additional processing, e.g. local contrasting. Pores near the external surface of the FE cylinder cladding are masked by a signal reflected from this surface. This is because of its large length along z axis.

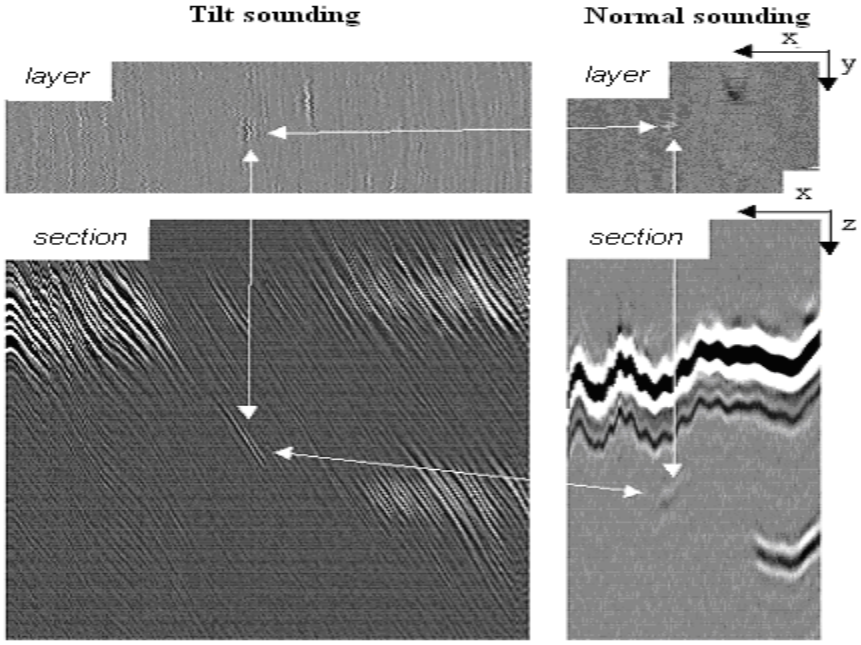

Fig.2. *Layer and section images according to inclined and normal sounding*

A section image obtained by means of oblique sounding has an absolutely different pattern. An image of local (point) irregularity can be observed as alternating dark and light slant lines. As in case of normal sounding, this is connected with oscillating nature of the reflected signal. Line slope is caused by the fact that during piezoelectric transducer movement and scanning along x axis the oblique distance from transducer to irregularities area (and the respective *z* delay) changes.
Images of external and internal fuel cladding surfaces look like a set of lines caused by reflections from the surface irregularities. As compared with normal sounding, the level of the signal reflected from the cylindrical surfaces is lower because only a part of energy reflected from irregularities having dimensions comparable with ultrasonic wavelength in water ($\lambda_w \approx 0,05$ mm) or in zirconium ($\lambda_z \approx 0.075$ mm) returns to the ultrasonic transducer. The most important advantage of oblique sounding is a very low reflection level in weld area because this makes it possible to detect pores near the external cladding surface boundary.
The section of incomplete penetration in the weld root looks also like a slant line. The characteristic feature of this slant line which allows to distinguish incomplete penetration from the pore consists in the following: In case of incomplete penetration the inclined line is positioned on the internal cylinder surface boundary in the area of

its contact with the end part. The important feature of incomplete penetration is its rather large length (as compared with the pore) along y-axis. This can be observed on layer and section images. On the layer images there are dark and light lines along y axis, on the section images – slant lines in a great number of sections (incomplete penetration in a form of arc) or in all sections (annular nonpenetration).

3. Description of algorithm for detection of pores and nonpenetrations and estimation of their dimensions and position: The features of weld defect images described in the previous sections were used for development of algorithms of defect detection using digital image processing. The image processing is performed to obtain brief description of defect area parameters and defect area coordinates as well as areas that circumscribe internal and external cylinder surfaces. Cylinder surface boundary control makes it possible to analyze only the image areas conforming to the weld zones. Moreover, the defect position relative to the surface boundaries can be used to distinguish the pores from the nonpenetrations. The processing consists of two steps.

I. Primary processing step – analysis of separate sections.

1. Sliding smoothing of images by columns of sections (according to time coordinate) using the following equation:

$$d^*(k,m,n) = \frac{1}{\Delta_{\tilde{n}}} \sum_{j=k-\Delta}^{k+\Delta} d(j,m,n), \qquad (1)$$

where $\Delta_{\tilde{n}} = (2\Delta + 1)$ – size of smoothing window in order to reduce structural interferences and quantization noise (It is assumed that $\Delta_{\tilde{n}} = 7$).

2. Formation of the 3-dimensional local variances array $D(k,m,n)$ in accordance with the below equation:

$$D(k,m,n) = \frac{1}{(2\Delta_k + 1)(2\Delta_m + 1)} \sum_{i=k-\Delta_k}^{k+\Delta_k} \sum_{j=m-\Delta_m}^{m+\Delta_m} d^{*2}(i,j,n) - \left\{ \frac{1}{(2\Delta_k + 1)(2\Delta_m + 1)} \sum_{i=k-\Delta_k}^{k+\Delta_k} \sum_{j=m-\Delta_m}^{m+\Delta_m} d^*(i,j,n) \right\}^2 . \qquad (2)$$

where $(2\Delta x + 1) \times (2\Delta y + 1)$ – the 2-dimensional window size, assumed 5×31 pixels. Procedures (1) and (2) correspond to square-law detection with the preliminary filtration and subsequent smoothing. Characteristic section image obtained by means of this processing is given in Fig. 3,a.

3. Detection of irregularities by binarization of the array $D(k,m,n)$ in accordance with the equation:

$$B(k,m,n) = \begin{cases} 1, & \text{ï ðè } D(k,m,n) > C \ \ (\text{î áúåêò}) \\ 0, & \text{ï ðè } D(k,m,n) \le C \ \ (\text{ôî í}), \end{cases}$$

where threshold C is determined adaptively by measuring of the array $D(k,m,n)$ histogram in the areas free from irregularities (in the end part area or inside the cladding behind the reflections from its internal surface), indicated by arrows in Fig. 2. The threshold is specified in such a way that the probability of threshold exceeding by the background counts doesn't exceed the tolerance. In experiments probability value is assumed equal to 0,005.

II. Secondary processing stage – analysis of primary processing results.

4. The obtained binary array is examined for all beams in the inclined direction in which the slant lines (at an angle of $-81,5^{\circ}$ relative to horizontal axis) are oriented. This results in compact representation of

slant lines as a set of numbers designating coordinates of (x_{st}, z_{st}) original and (x_{end}, z_{end}) end points as well as brightness value of center point and the section number m .

5. By comparison of different slant lines coordinates these slant lines are combined in the areas which are assigned individual numbers that are also included in description of each slant line.
6. Three coordinates of the mentioned area centers are determined as half-sums of the corresponding maximum and minimum coordinates of slant lines of this area and overall dimensions of the areas as well. The obtained area dimensions are considered as conditional defect dimensions.
7. The decision of defect existence is made. If the area dimensions exceed the predetermined value, the decision of pore existence is made. The decision on non-penetration is made in case of simultaneous fulfilment of two conditions: firstly, the distance between the area boundary circumscribing the internal cylinder surface and the analyzed area boundary shall be less than the threshold value; secondly, the length of this area along y axis shall be greater than the critical value determined on the basis of EB weld defect statistics and permissible dimensions of undetected nonpenetration.

The result of secondary stage processing of one section is presented in Fig. 3,b as a set of highlighted areas. Different brightness levels correspond to different areas. The external and internal cladding surface boundaries as well as pores shown as local areas of constant brightness are identified by means of analysis. The ultrasonic test results were compared with the results of metallographic analysis consisting in cutting of thin layers (about 0.1 mm) of cylindrical cladding along the x axis followed by a visual surface inspection. For analysis FEs were used that were welded with non-observance of technological process requirements and as a result of it the claddings had a great number of pores and nonpenetrations. Good agreement of computer processing and metallographic analysis results concerning both defect detection and defect coordinates determination was obtained during all experiments.

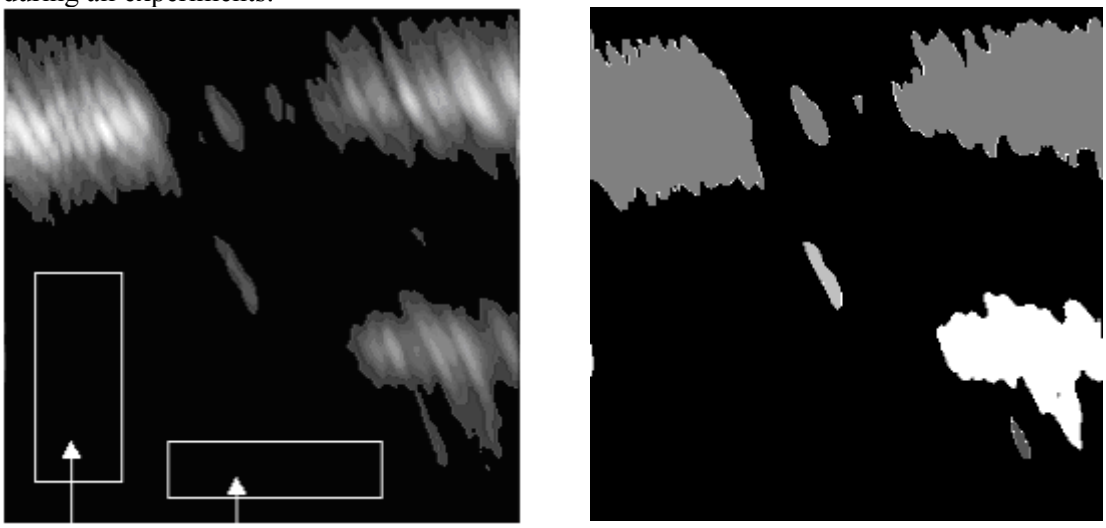

а б

Fig.3. *Pictures of local variances* $D(k, m = const, n)$ *and the binarization result*

4. Conclusion: The described results demonstrate high efficiency of ultrasonic test of the electron-beam welding quality using the oblique sounding. Suggested digital image processing algorithms make it possible to solve the main tasks of test automation.

The results of defect image size estimation obtained by use of suggested algorithms can be considered only as conditional estimates that show a monotonic dependence on real geometric dimensions. One way to plot such characteristic curves (calibration curves) is to produce artificial (model) defects of the given form and size in the FE weld seam area. It is rather a difficult task. Moreover, measuring problem becomes more complicated

due to ultrasonic transducer operation in the near zone and because of influence of FE surface and weld seam irregularities influence on the ultrasonic wave propagation picture. Further studies are required to solve this problem.